lubricants

MDPI

Article

Comparative Study of Tribological Behavior of Electroless Ni–B, Ni–B–Mo, and Ni–B–W Coatings at Room and High Temperatures

Arkadeb Mukhopadhyay [1], Tapan Kumar Barman [1], Prasanta Sahoo [1,*] and J. Paulo Davim [2]

[1] Department of Mechanical Engineering, Jadavpur University, Kolkata 700032, India; arkadebjume@gmail.com (A.M.); tkbarman@gmail.com (T.K.B.)

[2] Department of Mechanical Engineering, University of Aveiro, 3810-193 Aveiro, Portugal; pdavim@ua.pt

* Correspondence: psjume@gmail.com; Tel.: +91-33-2457-2660

Received: 6 July 2018; Accepted: 31 July 2018; Published: 2 August 2018

Abstract: Ni–B alloys deposited by the electroless method are considered to be hard variants of the electroless nickel family. Inclusion of Mo or W to form ternary alloys improves the thermal stability of electroless nickel coatings. Therefore, in the present work, Ni–B, Ni–B–Mo, and Ni–B–W coatings are deposited; and their tribological behavior at room and high temperatures are investigated. Electroless Ni–B, Ni–B–Mo, and Ni–B–W coatings are deposited on AISI 1040 steel substrates. The coatings are heat treated to improve their mechanical properties and crystallinity. Tribological behavior of the coatings is determined on a pin-on-disc type tribological test setup using various applied normal loads (10–50 N) and sliding speeds (0.25–0.42 m/s) to measure wear and coefficient of friction at different operating temperatures (25 °C–500 °C). Ni–B–W coatings are observed to have higher wear resistance than Ni–B or Ni–B–Mo coatings throughout the temperature range considered. Although for coefficient of friction, no such trend is observed. The worn surface of the coatings at 500 °C is characterized by lubricious oxide glazes, which lead to enhanced tribological behavior compared with that at 100 °C. A study of the coating characteristics such as composition, phase transformations, surface morphology, and microhardness is also carried out prior to tribological tests.

Keywords: electroless; Ni–B; Ni–B–W; Ni–B–Mo; COF; mass loss; high temperature

1. Introduction

Electroless nickel (EN) coatings are widely used in industries and investigated by researchers as a result of their excellent surface finish, corrosion resistance, wear resistance, and low coefficient of friction (COF) [1]. One of the principal advantages of coating deposition using the electroless method is the uniformity of deposits [2]. As a result of this, it becomes easier to coat complex shapes. Furthermore, the use of electricity is avoided. Electrons are provided by a reducing agent present in the electroless bath. Primarily, sodium hypophosphite or sodium borohydride is used as the reducing agent, which leads to deposition of Ni–P or Ni–B based coatings [3]. This facilitates coating of a variety of substrates that are not catalytically active [4]. A third element co-deposited along with Ni–P or Ni–B leads to the formation of ternary [5–9] or poly-alloy coatings [10–13]. The choice of the third element depends on the application for which the coating is required. Inclusion of Mo or W improves thermal stability of EN coatings, tribological characteristics, and corrosion resistance [14–18]. Inclusion of Cu also leads to an improvement in corrosion resistance [19]. Recently, EN nano-composites have gained attention because they exhibit improved hardness, corrosion resistance, and tribological characteristics compared with the alloy coatings [20–22]. However, research work is still ongoing to improve the properties of alloy coatings as a tough EN matrix is necessary to prevent delamination of composite particles [3].

The Ni–B alloy coating has higher wear resistance and low COF compared with Ni–P alloy [23]. This is attributed to the high hardness, self-lubricating microstructure and columnar growths [24]. Consequently, a reduction in the actual contact area takes place, thereby improving the tribological characteristics [25]. Suitable treatments of Ni–B coatings may even lead to microhardness that is equivalent to chromium [26]. As a result of this, Ni–B coatings are considered to be a suitable alternative to chromium, which has environmental concerns. Friction and wear characteristics of magnesium and aluminium alloys that are widely used commercially could be improved by Ni–B alloy deposition [27]. An improvement of tribological behavior of Ni–B coatings is also achieved on inclusion of W or Mo [28,29]. In fact, co-deposition of nano Al_2O_3 results in an increase in microhardness by ~290 HV_{100} [30]. The mass loss and COF of Ni–B–Al_2O_3 coatings is almost six and two times lower, respectively, in comparison with Ni–B alloy in as-deposited state. Similar results have been also observed on inclusion of B_4C nano-particles [31]. Impregnation of Ni–B coatings with PTFE (40%) results in a COF as low as <0.1 in non-lubricated, as well as 3.5% NaCl lubricated sliding condition [32]. Electroless Ni–B coatings have been applied in greaseless guns and barrel bores that are subjected to hostile environments proving to be a suitable replacement to chromium [33]. Recent studies have focused attention on duplex and multi-layer coatings that possess intermediate/enhanced tribological characteristics compared with the single layered binary alloys [34,35].

As Ni has a high melting point, the coatings may prove to be beneficial at high temperature sliding condition and demanding environments [36–39]. In fact, on heat treatment, the amorphous Ni–B coatings become crystalline and precipitation of hard boride (Ni_3B, Ni_2B) phases takes place [36–40]. These boride phases have a high melting temperature (~1150 °C). Hence, Ni–B coatings could be a suitable candidate up to 600 °C operating temperature. Pal et al. [40] observed that completely crystalline Ni–B coatings have the ability to retain their hardness at high temperatures of 100–400 °C. The friction and wear of Ni–B based coatings are governed by several factors at high temperature sliding condition such as formation of tribo-patches, phase transformations, microstructural changes, strain hardened debris, and so on [36–40]. In most of the research works, the tribological behavior of the coatings has been investigated individually [41–43]. The present work is therefore aimed at a systematic comparative study of tribological characteristics of the binary and ternary Ni–B based alloy coatings at room and high temperatures (100–500 °C). Tribological tests are carried out on a pin-on-disc configuration tribometer by varying the applied normal load (10–50 N) and sliding speed (0.25–0.42 m/s) at different operating temperatures. Electroless Ni–B based coatings are selected because they have been proven to have wear and friction reduction capabilities at ambient temperature. The tribological behavior of binary Ni–B is compared with ternary Ni–B–W and Ni–B–Mo coatings. The inclusion of W and Mo is considered because thermal stability of EN coatings is improved on the inclusion of W or Mo.

2. Materials and Methods

2.1. Deposition of Electroless Nickel Boron and Its Variants

The electroless bath in the present work is an alkaline bath with nickel chloride (20 g/L) as the source of nickel and sodium borohydride (0.8 g/L) as the reducing agent. For deposition of Ni–B–Mo and Ni–B–W, sodium molybdate (25 g/L) and sodium tungstate (25 g/L), respectively, are added. Suitable amounts of complexant, buffer, and stabilizers are also added. The bath composition is adopted as per a previous work,which gives 25-µm thick coatings [36]. The detailed composition and deposition condition may be found there [36]. A 200 mL bath volume with a double bath deposition system of 2 h each is adopted. Electroless Ni–B, Ni–B–Mo, and Ni–B–W coatings are deposited on AISI 1040 steel blocks of dimension of 20 mm × 20 mm × 2 mm for coating characterization. 'Pin' specimens with 6 mm diameter and 30 mm length are used for tribological characterization. The substrates used for coating deposition have centre line average roughness of 0.4 µm (N5 roughness grade). Prior to coating deposition, the specimens are rinsed thoroughly using deionized water and degreased in

acetone. Any oxide scales on the steel specimens are removed by dipping in 50% HCl solution. Finally, the specimens are again rinsed in deionized water. Post deposition duration of 4 h following a double bath system, the coated specimens are withdrawn from the bath, rinsed thoroughly in deionized water, and dried in air. The coated specimens are then heat treated in a muffle furnace for 1 h and allowed to cool inside the furnace itself. This is done to improve the mechanical properties of the coatings because heat treatment results in precipitation hardening of the deposits. It has been well established that precipitation of hard boride phases take place on heat treating borohydride reduced EN coatings. This leads to enhanced friction and wear characteristics compared with as-deposited condition. Electroless Ni–B and Ni–B–W coatings are heat treated at 350 °C because they exhibit high wear resistance and low COF at room, as well as high temperature sliding condition on heat treatment at 350 °C [37,38]. On the other hand, Ni–B–Mo coatings are heat treated at 350 °C for room temperature sliding wear tests and 450 °C for high temperature sliding wear tests. This is again based on a previous work carried out by Mukhopadhyay et al. [39] where Ni–B–Mo coatings heat treated at 350 °C and 450 °C revealed enhanced tribological characteristics at room and elevated temperatures, respectively.

2.2. Characterization of Nickel Boron and Its Variants

An energy dispersive X-ray (EDX) analyzer with Si (Li) super ultra-thin window (SUTW) that has the capability to transmit low energy X-rays is used to determine the coating composition. EDX analysis is carried out for the as-deposited Ni–B based alloys at a low accelerating voltage of 10 kV. Phase structure of the coatings is determined using X-ray diffraction (XRD) technique with a Cu Kα source (λ = 0.154 nm). Scanning speed of 1°/min and 2θ value ranging between 20–80° is taken for the analysis. Surface morphology of the heat treated coatings is observed under a scanning electron microscope (SEM), which has an Everhart Thornley secondary electron detector (Quanta FEG 250, FEI, Hillsboro, OR, USA). The centre line average roughness of the coatings is measured using a stylus type profilometer (Talysurf, Surtronic 3+, Taylor Hobson, Leicester, UK) set to 0.8 mm sampling length, 4 mm traverse length, 1 mm/s traverse speed, and Gaussian filter. The probe is equipped with a diamond tip of radius 5 µm. The results are processed using Talyprofile software (Taylor Hobson, Leicester, UK), which gives the centre line average roughness. The average of six readings is considered to evaluate the roughness of the coatings. Vicker's microhardness of the coatings is measured at an indentation load of 100 gf, dwell time of 15 s, and approach velocity of 25 µm/s. On the surface of the coatings, 10 indentations are considered to measure the microhardness.

2.3. Tribological Characterization of Nickel Boron and Its Variants

Friction and wear characteristics of heat treated Ni–B, Ni–B–Mo, and Ni–B–W coatings are determined on a pin-on-disc type tribological test setup. Coated pin specimens slides against a rotating EN 31 steel counterface disc. Tribological tests are carried out at room temperature (25 °C), 100 °C, 300 °C, and 500 °C. For high temperature tests, the counterface disc is heated up to the desired temperature using a 15 kVA high frequency induction heating arrangement. The operating temperature is continuously monitored using a pyrometer having an accuracy of 1 $\pm$ 1% of measured value of temperature. Applied normal load and sliding speed is varied as indicated in Table 1. Test duration is held constant at 300 s. Experiments are carried out for all possible combination of the parameters laid down in Table 1. Frictional force is acquired using a button type load cell with an accuracy of 0.1 $\pm$ 1% of measured value of force. Wear is evaluated from the mass loss of the coatings using a high precision weighing balance having a readability of 0.01 mg. Wear mechanism and worn surfaces are characterized using SEM and EDX for the highest level combination of applied normal load and speed, that is, 50 N and 0.42 m/s, respectively.

Table 1. Tribological test parameters.

Parameters	Levels				
	1	**2**	**3**	**4**	**5**
Load (N)	10	30	50	×	×
Sliding speed (m/s)	0.25	0.29	0.33	0.38	0.42
Temperature (°C)	25	100	300	500	×
Test duration = 300 s					

3. Results and Discussion

3.1. Composition, Structure, and Surface Morphology of Nickel Boron and Its Variants

Coating composition in terms of weight percentage of Ni, B, W, and Mo is given in Table 2 and is determined using EDX analysis. From the B content, it is seen that the coatings lie in the mid-B range [34]. Inclusion of Mo does not cause a significant change in coating composition, but a slight decrease in B content takes place due to the inclusion of W. The deposition of Mo in the coatings is higher compared to W even though the concentration of sodium molybdate and tungstate is same in the coating bath. This is due to the fact that Mo (VI) species exist as MoO_4^{2-} while W (VI) species exist as cluster of complex ions [36]. This result in higher deposition of Mo compared with W in the coatings.

Table 2. Energy dispersive X-ray (EDX) analysis of Ni–B, Ni–B–Mo, and Ni–B–W coatings.

Elements	Weight Percentage in Different Coatings		
	Ni–B	**Ni–B–Mo**	**Ni–B–W**
Ni	94.5	90.7	91.4
B	5.5	5.4	5.2
W	×	×	3.4
Mo	×	3.9	×

The coatings in as-deposited condition are generally found to be amorphous [36–39]. XRD results of heat treated Ni–B and Ni–B–W coating at 350 °C for 1 h are shown in Figure 1. Heat treatment results in precipitation of Ni_3B and Ni_2B phases along with Ni (111). Similar results have also been obtained for Ni–B–Mo coatings heat treated at 350 °C, as can be seen in Figure 2. Although, stable Ni_3B phases are observed along with Ni (111) on heat treating Ni–B–Mo coating at 450 °C for 1 h. Precipitation of hard boride phases on heat treating Ni–B and its variants has been also reported in the literatures [23–29].The analysis of XRD results is presented in Table 3. The procedure for calculation of absolute integrated intensity of peaks and crystallite size is mentioned elsewhere [13,40]. The highest intensity peak in Figure 1a corresponds to Ni (111), which is also superimposed with Ni_2B. In the case of Ni–B–W coatings, the highest intensity peak shifts to ~44.9° and corresponds to Ni (111). Similar results are observed for Ni–B–Mo coatings heat treated at 350 °C or 450 °C for 1 h, where the highest intensity peak is observed at ~44.7° corresponding to Ni (111). The analysis in Table 3 is based on the highest intensity peak of Ni (111) and Ni_3B peak, which follows after it as they are consistent in Figure 1 as well as Figure 2. The crystallite size of Ni (111) is the highest for Ni–B–Mo coatings and the lowest for Ni–B coating. The absolute integrated intensity of the peaks is also given in Table 3. From the analysis, it can be seen that as Ni–B–Mo coatings are heat treated at 450 °C for 1 h, the absolute integrated intensity of Ni (111) increases, while that of Ni_3B decreases. This is consistent with other research works [40] and may happen because of inter-diffusion of B into the substrate. A significant change in crystallite size of Ni (111) or Ni_3B is not observed though. Further, a coarser grained structure is observed for Ni–B–Mo coatings.

Surface morphology of Ni–B and Ni–B–W coatings after heat treatment at 350 °C for 1 h is shown in Figure 3. The surface of heat treated Ni–B coating typically resembles a cauliflower-like nodular

morphology with distinct cellular boundaries. This cauliflower-like morphology is responsible for excellent anti-friction characteristics of Ni–B coatings. In fact, Ni–B–W coatings also present a compact and nodulated morphology in Figure 3b. SEM micrographs of Ni–B–Mo coating post heat treatment at 350 °C and 450 °C are shown in Figure 4. The surface appears to be quite coarse in the case of Ni–B–Mo coating heat treated at 350 °C (Figure 4a) with cellular boundaries. On heat treatment at 450 °C for 1 h, oxide scales can be observed on the surface of Ni–B–Mo coating in Figure 4b. The nodulated structures also grow in size, indicating grain growth and an increase in degree of crystallization.

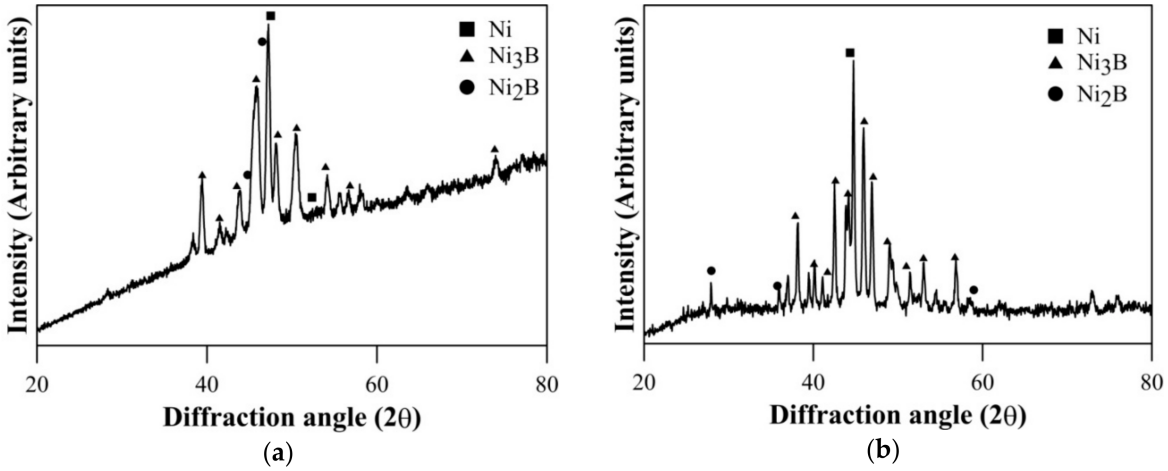

Figure 1. X-ray diffraction (XRD) results of heat treated (**a**) Ni–B and (**b**) Ni–B–W coating at 350 °C for 1 h.

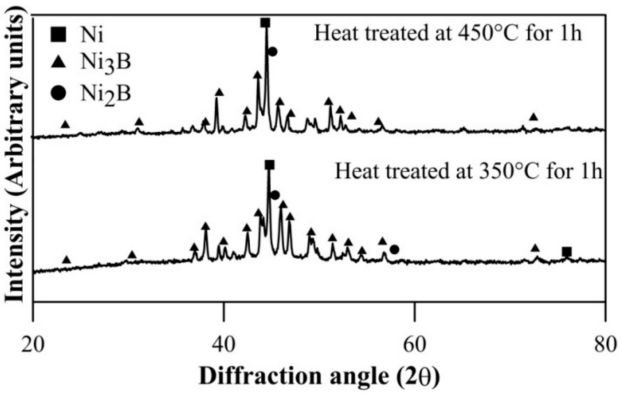

Figure 2. XRD results of electroless Ni–B–Mo coating heat treated at 350 °C and 450 °C for 1 h.

Table 3. XRD results analysis of Ni–B, Ni–B–W, and Ni–B–Mo coatings.

Coating	Peak Position (2θ)		Absolute Integrated Intensity (au)		Crystallite Size (nm)	
	Ni	Ni_3B	Ni	Ni_3B	Ni	Ni_3B
Ni–B (350 °C)	46	47	2455	2014	18.1	18.15
Ni–B–W (350 °C)	44.9	45.95	715	639	38.2	26.64
Ni–B–Mo (350 °C)	44.7	46	1892	1209	51	24.96
Ni–B–Mo (450 °C)	44.7	45.85	2268	708	51	23.81

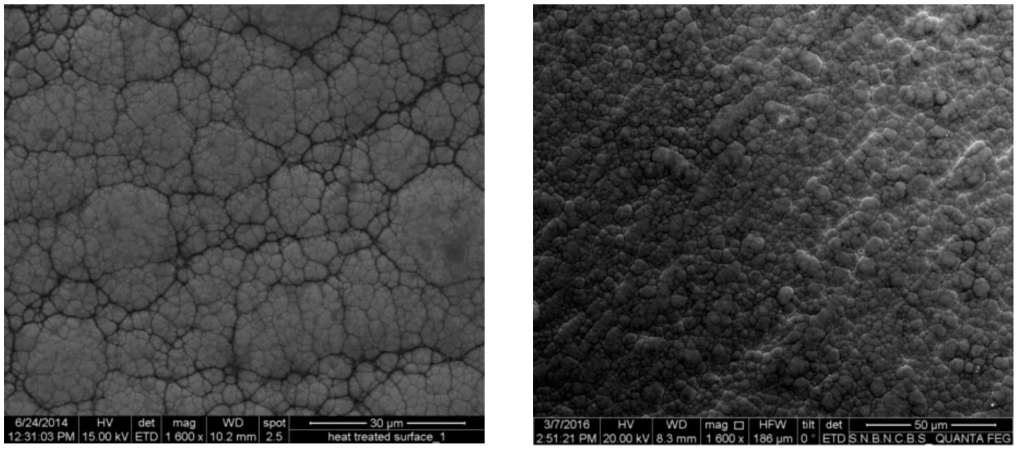

(**a**) (**b**)

Figure 3. Surface morphology of (**a**) Ni–B and (**b**) Ni–B–W coating post heat treatment at 350 °C for 1 h.

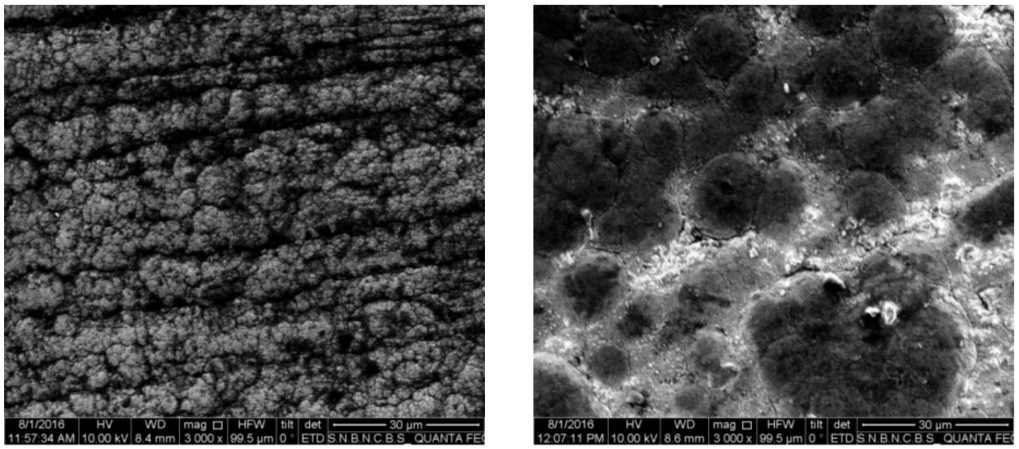

(**a**) (**b**)

Figure 4. Scanning electron microscope (SEM) micrograph of Ni–B–Mo coating heat treated at (**a**) 350 °C and (**b**) 450 °C for 1 h.

The centre line average roughness (R_a) of the coatings is laid down in Table 4. Electroless Ni–B–W coatings exhibit lowest roughness, while Ni–B–Mo exhibit the highest. Ni–B coatings have R_a intermediate to that of Ni–B–W and Ni–B–Mo coatings. The R_a values also indicate a coarse morphology of Ni–B–Mo coatings, observed in Figure 4, in comparison with Ni–B or Ni–B–W coatings (Figure 3). Therefore, the SEM and roughness results corroborate well with each other. Furthermore, the roughness of Ni–B and Ni–B–W coatings are close to the substrate, which is attributed to the fact that EN coatings follow the substrate roughness. The R_a of Ni–B–Mo coating is significantly higher on heat treatment at 450 °C because of the formation of oxide scales along with grain coarsening.

Table 4. Surface roughness of Ni–B, Ni–B–Mo, and Ni–B–W coatings.

Coating	Surface Roughness, R_a (µm)	
	Heat Treated at 350 °C	Heat Treated at 450 °C
Ni–B	0.66	-
Ni–B–Mo	0.76	0.87
Ni–B–W	0.46	-

3.2. Microhardness of Nickel Boron and Its Variants

Vicker's microhardness of the coatings is given in Table 5. A high microhardness is observed for the coatings heat treated at 350 °C for 1 h and is attributed to the precipitation hardening phenomenon. Electroless Ni–B–W coatings possess higher hardness due to solid solution strengthening caused by the inclusion of W [28,38]. The microhardness of Ni–B–Mo coatings is lower compared with Ni–B or Ni–B–W coatings. This is attributed to the coarse grained morphology of Ni–B–Mo coating in comparison with Ni–B or Ni–B–W (Figures 3 and 4). Such coarse grain morphology may arise when Mo is co-deposited as a result of its higher growth stresses [36]. When Ni–B–Mo coatings are heat treated at 450 °C, a significant change in microhardness is not observed. This could be an indication of higher thermal stability of the deposits [29,39]. High microhardness of heat treated Ni–B and its ternary variants are in accordance with the literature [23–29].

It should be noted here that coating hardness was measured using Vicker's micro-indentation rather than nano-indentation technique. The microhardness results presented in Table 5 correspond to a diagonal length of ~13 to 18 μm. From the diagonal length, the indentation depth is estimated to be ~4 to 6 μm. As the thickness of the coatings in the present work is 25 μm, the indentation depth is accordingly estimated to be about 16% of the coating thickness. This may affect the hardness results by introducing the effect of substrate as reported in other research works [44–46].The indentation depth is recommended to not exceed 1/10 of the measured coating thickness [44–46]. Therefore, for thin coatings, it is always suitable to address nano-hardness instead of micro-hardness, keeping in mind the thickness of the films. While EN coatings have been widely characterized by the micro-indentation technique in other research works [23,25], the microhardness results reported in Table 5 are in line with them. Furthermore, as the present work considers a similar group of coatings and their comparative study with consistent indentation depth for all the three variants, the results are comparable within the coating groups.

The elastic modulus of the coatings has a significant effect on the tribological behavior of the coatings. Such observations have been made in recent studies from nano-indentation tests [15,24,40]. It may be obtained from depth of indentation after removal of the indenter [44]. Pal et al. [40] reported that completely crystalline Ni–B coatings have the ability to retain their elastic modulus even at high temperatures of 100–400 °C. Nano-indentation responses, as well as the elastic modulus of the coatings at elevated temperatures, may be addressed in future research works.

Table 5. Microhardness of Ni–B, Ni–B–Mo, and Ni–B–W coatings.

Coating	Microhardness (HV_{100})	
	Heat Treated at 350 °C	**Heat Treated at 450 °C**
Ni–B	1060 ± 20	×
Ni–B–Mo	738 ± 20	690 ± 20
Ni–B–W	1181 ± 20	×

3.3. Tribological Behavior of Nickel Boron and Its Variants at Room Temperature

Mass loss of borohydride reduced EN coatings at room temperature is presented in Figure 5. With an increase in applied normal load, the increase in mass loss is quite significant for Ni–B coating compared with Ni–B–Mo or Ni–B–W coatings. Furthermore, at 50 N load, mass loss of Ni–B coatings shows a steep rise. It is also observed in Figure 5 that wear resistance of Ni–B–W coating at room temperature is the highest in comparison with Ni–B or Ni–B–Mo coatings owing to its high hardness. Although the microhardness of Ni–B coatings is higher in comparison with Ni–B–Mo coatings, wear of Ni–B coatings is still found to be higher. The boride phases, along with the presence of Mo, may lead to enhanced wear resistance of Ni–B–Mo in comparison with the binary Ni–B alloy [15].

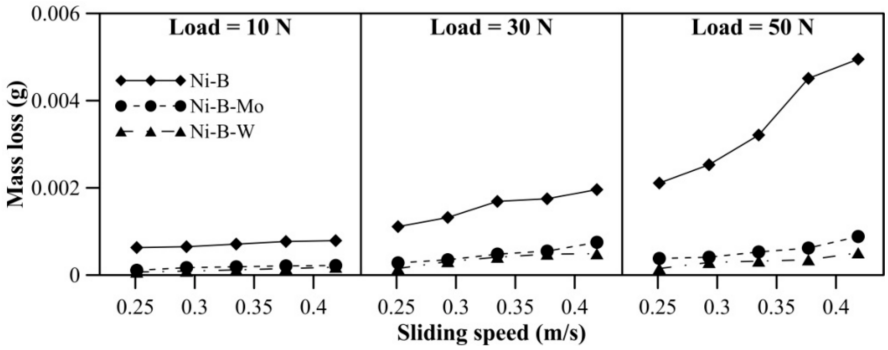

Figure 5. Wear behavior of nickel boron and its variants at room temperature.

The COF of Ni–B, Ni–B–Mo, and Ni–B–W coatings can be observed in Figure 6. The COF of Ni–B–W coating increases significantly with load. The coatings do not exhibit significant variation in COF with speed. A reversal in trend for COF is observed, that is, Ni–B–W coatings exhibit the highest COF, followed by Ni–B–Mo and Ni–B (Figure 6). Even though heat treatment improves microhardness and wear resistance of Ni–B–W coatings, it also facilitates diffusion of W to coating surface through the cellular boundaries [28,38]. Oxides of W are generally found to be brittle at room temperature, which in turn increases COF of Ni–B–W coating [47]. Thus, wear resistance improves but COF deteriorates in the case of Ni–B–W coatings. Ni–B–Mo coatings exhibit higher COF in comparison with Ni–B, even though the wear resistance of Ni–B–Mo is higher than Ni–B alloy. This may be attributed to the coarse morphology and higher roughness as observed in Figure 4a.

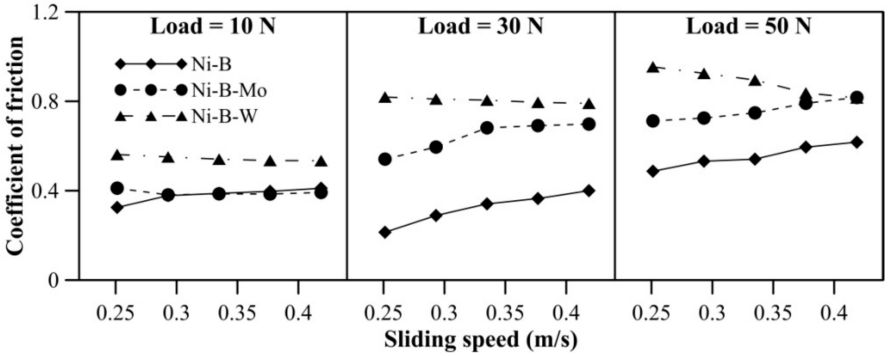

Figure 6. Coefficient of friction (COF) of nickel boron and its variants at room temperature.

Worn surfaces of the coatings at the highest level of load (50 N) and speed (0.42 m/s) at room temperature is illustrated in Figure 7. Ploughing and scratches on the Ni–B coating is observed in Figure 7a accompanied by the formation of cracks. It could be well observed in Figure 7b that the wear track is filled with fine and some coarse debris particles scattered on the wear track of Ni–B–Mo coatings. These fine particles have a self lubricating effect, leading to the low wear of the coatings. However, some of the coarse ones present may tend to increase the COF. In the case of Ni–B–W coating (Figure 7c), the worn surface appears to be comparatively smoother and characterized by flattened nodules. Thus, wear is significantly higher for Ni–B coatings in comparison with Ni–B–Mo or Ni–B–W. The wear mechanism observed in Figure 7 could be another reason for Ni–B–Mo coatings exhibiting tribological characteristics intermediate to Ni–B and Ni–B–W.

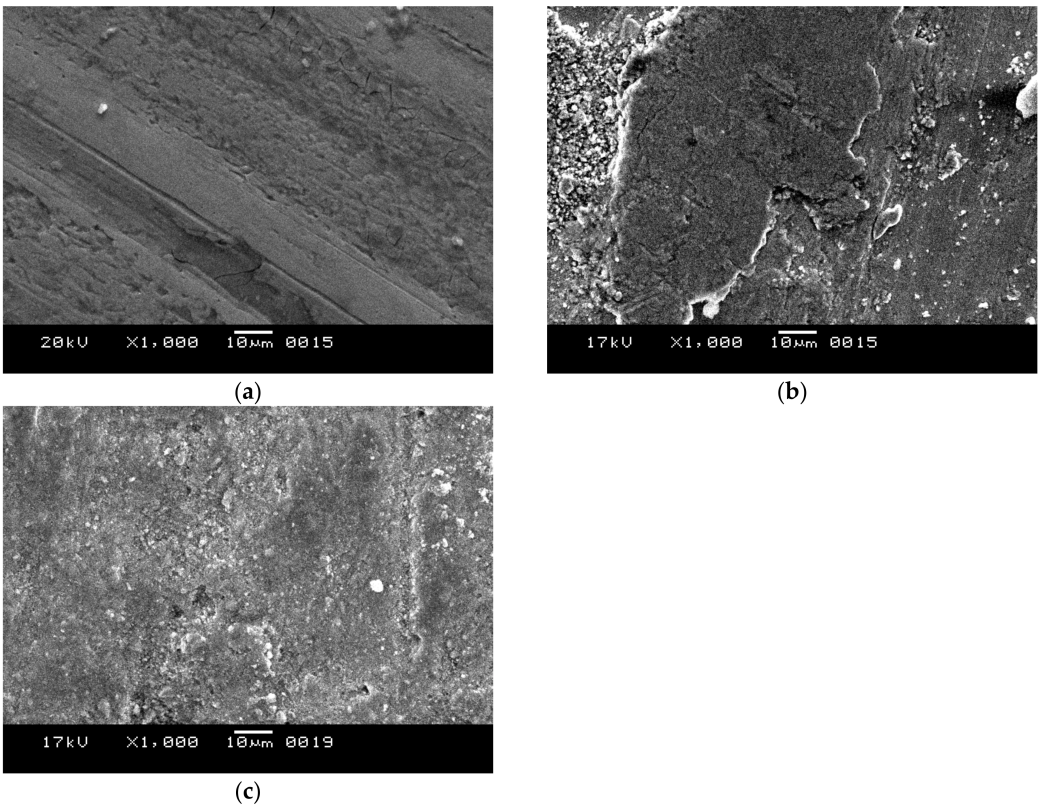

Figure 7. Worn surface of (**a**) Ni–B, (**b**) Ni–B–Mo, and (**c**) Ni–B–W coatings at 50 N load, 0.42 m/s speed, and room temperature operating conditions.

3.4. Tribological Behavior of Nickel Boron and Its Variants at 100 °C

Wear behavior of the coatings at 100 °C can be observed in Figure 8. The mass loss of Ni–B coatings increases with load, as well as sliding speed. Compared with 10 N, mass loss at 30 or 50 N is higher for Ni–B–Mo and Ni–B–W coatings. At 100 °C, the highest wear resistance is observed for Ni–B–W coatings, followed by Ni–B–Mo and Ni–B. The high wear resistance of Ni–B–W coatings at 100 °C is again attributed to its high hardness. The COF of Ni–B, Ni–B–Mo, and Ni–B–W coatings at 100 °C operating temperature can be observed in Figure 9. The COF of the coatings increases with an increase in sliding speed (Figure 9). With an increase in load from 10 N to 30 N, the COF of the coatings increases. Although at 50 N, the COF decreases in comparison with 10 or 30 N load. It may be also deduced that Ni–B–W coatings show high COF at 100 °C, and Ni–B–Mo show the lowest COF, particularly at high load and speed.

Wear surface morphology of Ni–B, Ni–B–Mo, and Ni–B–W coatings at 50 N, 0.42 m/s and 100 °C is shown in Figure 10. The worn surface of Ni–B coating is characterized by deep grooves caused by the ploughing action of strain hardened debris (Figure 10a). SEM micrograph of worn surface of Ni–B–Mo coating reveals plastically deformed patches and a deep crater (Figure 10b). In the case of Ni–B–W coatings, plastically deformed and broken nodules and loose scattered debris are present on the worn surface (Figure 10c). These broken nodules are smeared on other parts of the coating. The higher wear of Ni–B or Ni–B–Mo in comparison with Ni–B–W may be attributed to the strain hardened debris cutting through the softer EN matrix leading to partial delamination of the coatings at high load and speed. In the case of Ni–B–W coatings, mainly the coatings are plastically deformed and ground severely by the counterface disc, as observed in Figure 10c. Although no delamination of Ni–B–W coatings is observed. This again reveals higher wear resistance of Ni–B–W in comparison with Ni–B or Ni–B–Mo. The embrittlement of Ni–B–W coatings due to formation of WO_x could lead to higher COF and cracks (Figure 10c). Thus, at 100 °C, the highest wear resistance is concluded

for Ni–B–W coating. If both the properties are desired simultaneously, Ni–B–Mo is observed to be a suitable candidate in comparison with Ni–B or Ni–B–W.

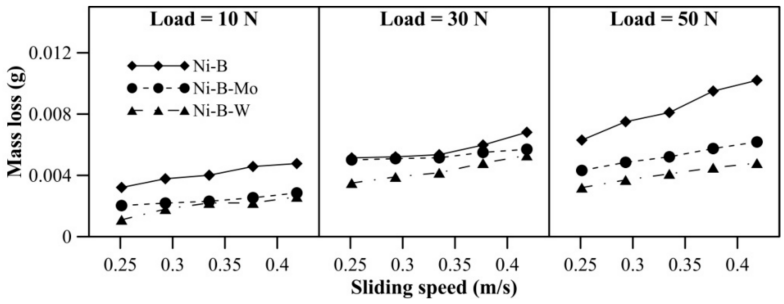

Figure 8. Wear behavior of nickel boron and its variants at 100 °C.

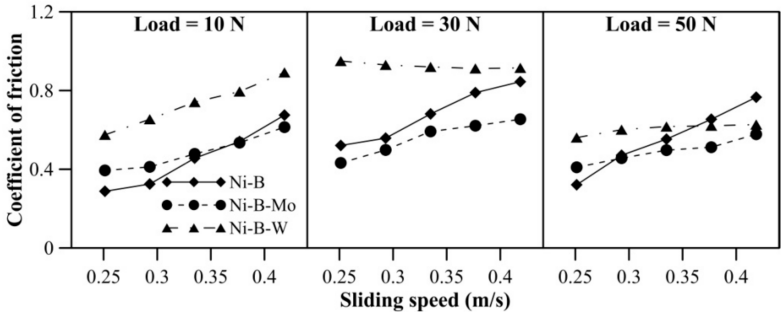

Figure 9. COF of nickel boron and its variants at 100 °C.

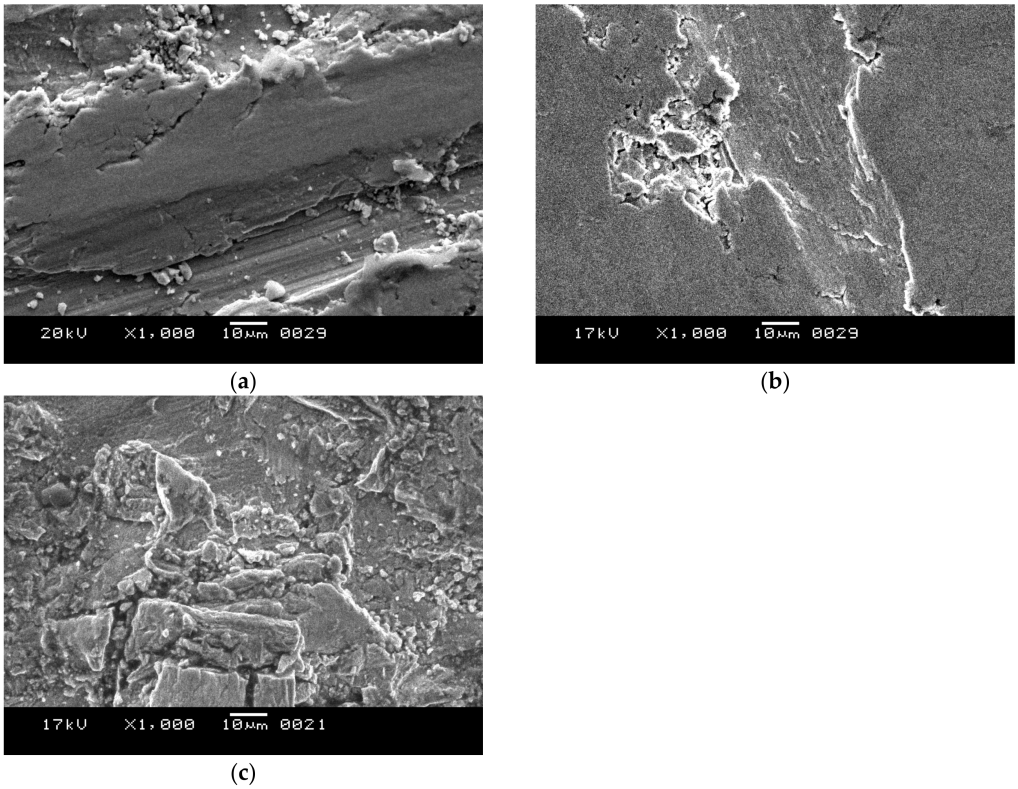

(**a**) (**b**) (**c**)

Figure 10. Worn surface of (**a**) Ni–B, (**b**) Ni–B–Mo, and (**c**) Ni–B–W coatings at 50 N load, 0.42 m/s speed, and 100 °C operating conditions.

3.5. Tribological Behavior of Nickel Boron and Its Variants at 300 °C

The wear characteristics of borohydride reduced EN alloy coatings at 300 °C can be observed in Figure 11. With an increase in load, mass loss of Ni–B–Mo coatings increases significantly. In the case of Ni–B coatings, mass loss decreases at 50 N in comparison with 30 N. Similar behavior is also observed for Ni–B–W coating. The mass loss of Ni–B and Ni–B–W coatings increases with an increase in speed from 0.25 m/s to 0.33 m/s at all values of normal loads. Although mass loss again decreases at 0.38 m/s and 0.42 m/s. Wear resistance of Ni–B–W coatings is the highest at 300 °C, while that of Ni–B–Mo is the lowest. The COF of the coatings at 300 °C can be observed in Figure 12. The COF of the coatings do not exhibit significant variation with applied normal load and speed. The COF of Ni–B–Mo coating is higher than Ni–B or Ni–B–W coating, especially at 50 N.

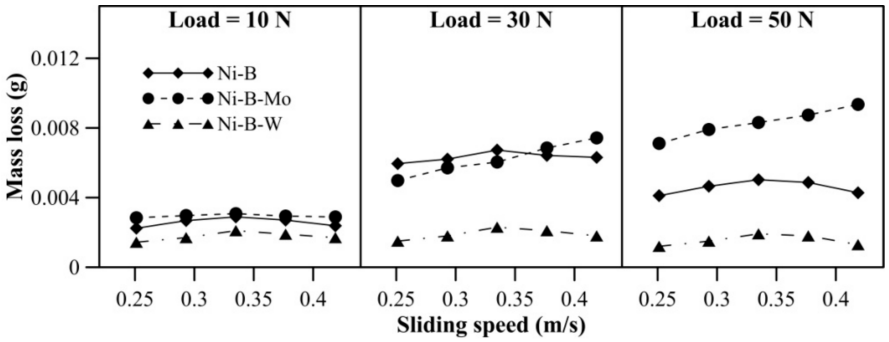

Figure 11. Wear behavior of nickel boron and its variants at 300 °C.

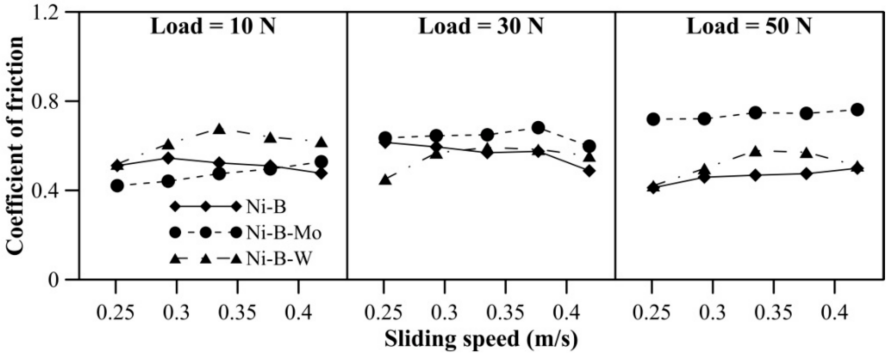

Figure 12. COF of nickel boron and its variants at 300 °C.

SEM micrographs of the worn surface of Ni–B, Ni–B–Mo, and Ni–B–W coatings at 300 °C are shown in Figure 13. The worn surface of Ni–B coating appears smooth with flattened patches and microgrooves along the sliding direction (Figure 13a). The mechanical properties of Ni–B–Mo coating seem to deteriorate and the worn surface is characterized by coating delamination and an increase in adhesive component (Figure 13b). The worn surface of Ni–B–W coating is characterized by smeared nodules and scattered oxidized debris (from EDX analysis) (Figure 13c). The smeared patches are tribo-oxidative patches, which improves the tribological behavior of Ni–B–W coating. An increase in adhesive component leads to a significant increase in wear of Ni–B–Mo coatings in comparison with Ni–B or Ni–B–W, because their worn surfaces are characterized by flattened coating patches and act as load bearing areas. Consequently, COF of Ni–B and Ni–B–W coatings also show an improvement in comparison with Ni–B-Mo. In fact, Ni–B coatings exhibit superior anti-friction characteristics at 300 °C. Therefore, based on high wear resistance, Ni–B–W coating is suggested, while Ni–B is suggested for anti-friction applications at 300 °C. Considering the overall performance at 300 °C test temperature, if both wear resistance and low COF are desired, the use of Ni–B–W coating is suggested.

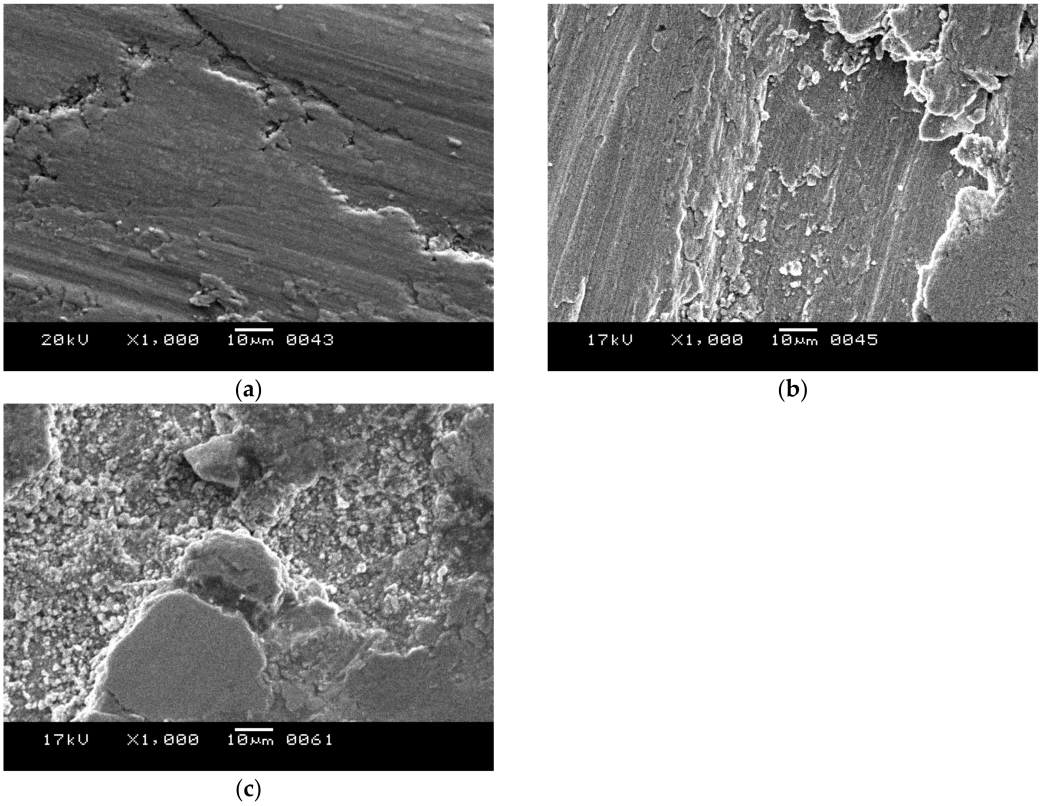

Figure 13. Worn surface of (**a**) Ni–B, (**b**) Ni–B–Mo, and (**c**) Ni–B–W coatings at 50 N load, 0.42 m/s speed, and 300 °C operating conditions.

3.6. Tribological Behavior of Nickel Boron and Its Variants at 500 °C

Wear behavior of borohydride reduced coatings at 500 °C is shown in Figure 14. With an increase in applied normal load, the mass loss of Ni–B and Ni–B–Mo coatings increases. While for Ni–B–W coatings, the mass loss at 10 N and 30 N is almost similar, but increases at 50 N. With sliding speed, mass loss of Ni–B and Ni–B–W coating increases, but a curvature is observed in the case of Ni–B–Mo coatings. Within 0.25–0.33m/s, mass loss of Ni–B–Mo coating increases and from 0.38m/s onwards, it starts decreasing again. The COF of the coatings at 500 °C is shown in Figure 15. The COF of Ni–B, Ni–B–Mo, or Ni–B–W coatings do not show a significant variation with load and speed at 500 °C. Wear tracks of the coatings are presented in Figure 16. The worn surface of Ni–B coating consists of smooth and lubricious oxide glazes of Ni (Figure 16a), while that of Ni–B–Mo consists of oxides of Mo and Ni (Figure 16b). In the case of Ni–B–W coatings, oxide glazes of Ni and W are formed (Figure 16c). The formation of oxide glazes is mainly deduced from the EDX point analysis.

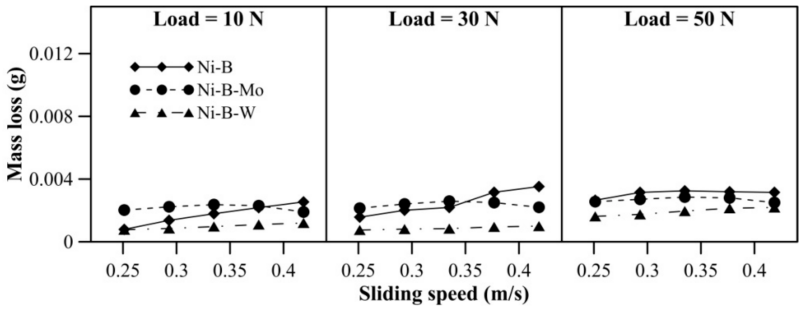

Figure 14. Wear behavior of nickel boron and its variants at 500 °C.

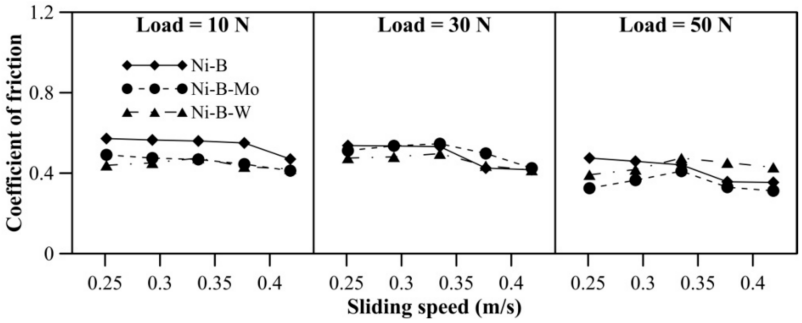

Figure 15. COF of nickel boron and its variants at 500 °C.

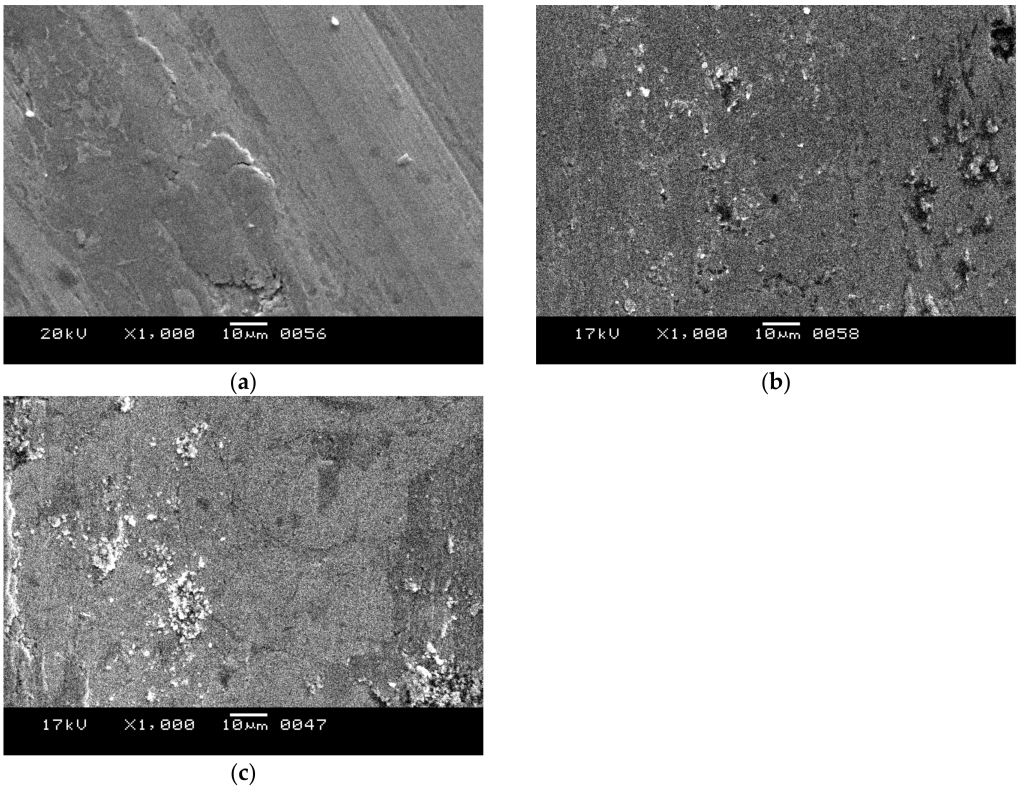

Figure 16. Worn surface of (**a**) Ni–B, (**b**) Ni–B–Mo, and (**c**) Ni–B–W coatings at 50 N load, 0.42 m/s speed, and 500 °C operating conditions.

Ni–B–W coatings exhibit excellent wear resistance in comparison with Ni–B or Ni–B–Mo coatings at 500 °C. Inclusion of W or Mo raises the crystallization temperature of Ni–B coatings [36–39]. Naturally, complete crystallization of the coatings is delayed. Microstructural changes result in toughening of Ni–B–W; and Ni–B–Mo coating facilitating support of the oxide patches and an improved wear resistance than the binary Ni–B alloy. At high temperatures, WO_x and MoO_x offer self-lubricating capabilities in comparison with room temperature conditions [47]. Therefore, at 500 °C, Ni–B–W as well as Ni–B–Mo exhibit low COF. Nevertheless, a very high COF of Ni–B coating is also not observed. Therefore, it is concluded that Ni–B–W coatings are suitable at 500 °C, considering both high wear resistance as well as low COF.

3.7. Effect of Temperature on Tribology of Nickel Boron and Its Variants

The effect of operating temperature on wear and friction characteristics of the coatings is presented in Figures 17 and 18, respectively, at lower level (10 N, 0.25 m/s), mid level (30 N, 0.33 m/s), and

the highest level (50 N, 0.42 m/s) of combination of load and speed. It can be seen that mass loss of Ni–B, Ni–B–Mo, and Ni–B–W coating shows a steep rise when the operating temperature is raised from room temperature to 100 °C. At 100 °C, the wear behavior is characterized by strain hardened debris cutting through the coating producing deep grooves, as well as delamination as can be seen in Figure 10. In fact, mass loss of Ni–B and Ni–B–W coatings tend to decrease at 300 °C or 500 °C in comparison with 100 °C. This happens as a result of the formation of oxide glazes and flattened patches that act as load bearing areas (Figures 13 and 16). Whereas mass loss of Ni–B–Mo coating increases further at 300 °C in comparison with 100 °C, and at 500 °C, again the mass loss decreases because of formation of MoO_x with self-lubricating capabilities [43]. It may be finally concluded that based on wear characteristics, Ni–B–W possess superior wear resistance in comparison with Ni–B or Ni–B–Mo throughout the temperature range. The COF of Ni–B–W or Ni–B–Mo coatings do not indicate significant variation with temperature at the lowest level of load and speed (10 N, 0.25 m/s), but in the case of Ni–B coating, COF increases with an increase in operating temperature. At the highest level of load and speed (50 N, 0.42 m/s), COF of Ni–B and Ni–B–W coating decreases at 300 °C or 500 °C in comparison with 100 °C. However, COF of Ni–B–Mo coating increases at 300 °C and decreases at 500 °C, especially at mid-level and the highest level of combination of load and speed. The COF of Ni–B–Mo coating at 300 °C is higher compared with 500 °C as a result of the formation of adhesion patches as can be seen in Figure 13b.

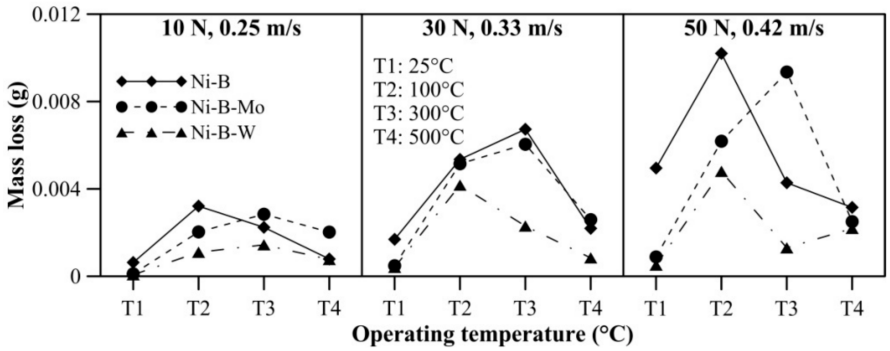

Figure 17. Effect of operating temperature on wear behavior of nickel boron and its variants.

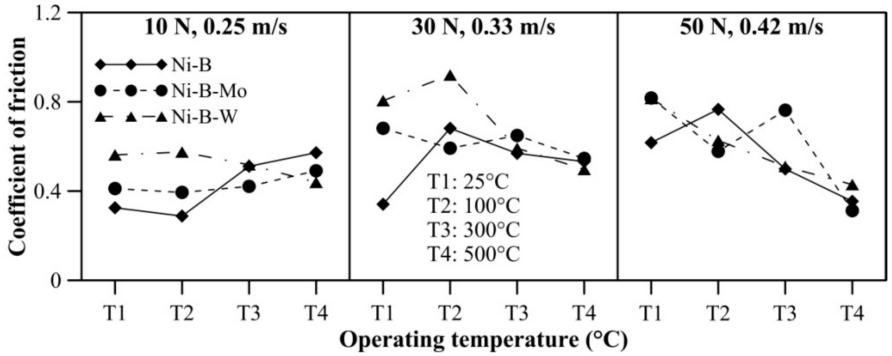

Figure 18. Effect of operating temperature on COF of nickel boron and its variants.

3.8. Selection of the Coatings Based on Tribological Behavior

At room temperature, Ni–B–W coatings exhibit high wear resistance, while Ni–B shows low COF. Considering both wear and COF, Ni–B–Mo coatings are suggested. Further, at 100 °C, high wear resistance is observed for Ni–B–W coatings, while a low COF for Ni–B–Mo coatings is observed. Overall, enhanced tribological behavior is concluded for Ni–B–Mo coatings at 100 °C. At 300 °C, high wear resistance is observed for Ni–B–W, while the binary Ni–B alloy shows low COF. Ni–B–W

coating is suggested based on overall performance at 300 °C. At 500 °C, Ni–B–W coatings show better tribological characteristics in respect of both high wear resistance and low COF. However, if the entire operating temperature range is considered, that is, 25 °C–500 °C, then Ni–B–W coatings would be preferable.

4. Conclusions

The present work considers the deposition of electroless Ni–B, Ni–B–Mo, and Ni–B–W coatings and their tribological characterization at room and high temperatures. Coatings are deposited on AISI 1040 steel substrates. The following conclusions may be directly drawn from the study:

- EDX analysis of the as-deposited coatings reveals that the deposits lie in the mid-B range (within 5–6 wt % B).
- To improve the mechanical properties of the coatings, they are heat treated. XRD analysis of the heat treated coatings indicates the precipitation of crystalline Ni (111) and boride phases.
- SEM micrograph of the heat treated coatings show that the surface is characterized by nodulated self-lubricating structures. Ni–B–Mo coatings present a coarse morphology with visible cellular boundaries; whereas Ni–B–W coatings have a densely nodulated morphology. The surface of Ni–B coating resembles cauliflower like morphology, which is common in borohydride reduced coatings.
- Because of precipitation of hard boride phases, a high microhardness of the coatings is observed on heat treatment. Ni–B–W coatings exhibit the highest microhardness followed by Ni–B and Ni–B–Mo coatings. Because of the coarse structure, Ni–B–Mo coatings have lower microhardness compared with Ni–B or Ni–B–W.
- The heat treated coatings are subjected to tribological tests at room and elevated temperatures of 100 °C, 300 °C, and 500 °C. For the temperature range considered, Ni–B–W coatings exhibit the highest wear resistance. Based on COF, Ni–B coatings exhibit lower values at room temperature, Ni–B–Mo at 100 °C, and Ni–B at 300 °C.
- At the highest value of test temperature, that is, 500 °C, almost all the three coatings exhibit similar values of COF. Although if one coating among the three has to be selected, Ni–B–W would be a suitable option.
- Ni–B–W coatings show higher COF at room temperature or 100 °C, but it improves at 300 °C or 500 °C. This is due to the fact that oxides of tungsten tend to be brittle at room temperatures, but have a lubricating effect at high temperatures.
- The wear mechanism also varies at different temperatures for Ni–B, Ni–B–Mo,or Ni–B–W coatings. In fact, the tribological behavior, wear mechanisms, and microstructural changes are inter-related.

From the present work, it would be possible to judge the suitability of borohydride reduced coatings for high temperature applications. Depending on the requirement such as anti-wear, anti-friction, or both, it would be possible to select the suitable alloy. Future research work may be carried out to evaluate the mechanical properties of the coatings at high temperature using nano-indentation techniques, which would further shed light on the tribological characteristics of the coatings. Profilometry techniques may be employed to evaluate the specific wear rate or wear coefficient of the coatings at high temperature.

Author Contributions: Conceptualization, P.S. and J.P.D.; Investigation, A.M. and T.K.B.; Writing—Original Draft Preparation, A.M.; Writing—Review & Editing, T.K.B., P.S., and J.P.D.

Funding: This research received no external funding.

Acknowledgments: The authors gratefully acknowledge the assistance of DST, PURSE-II program and COE, TEQIP-II program of Jadavpur University, Kolkata, India.

Conflicts of Interest: The authors declare no conflict of interest.

References

1. Sahoo, P.; Das, S.K. Tribology of electroless nickel coatings—A review. *Mater. Des.* **2011**, *32*, 1760–1775. [CrossRef]
2. Duari, S.; Mukhopadhyay, A.; Barman, T.K.; Sahoo, P. Tribological performance optimization of electroless nickel coatings under lubricated condition. In *Design and Optimization of Mechanical Engineering Products*; Kumar, K., Davim, J.P., Eds.; IGI Global: Hershey, PA, USA, 2018; pp. 250–280.
3. Mukhopadhyay, A.; Barman, T.K.; Sahoo, P. Electroless nickel coatings for high temperature applications. In *Composites and Advanced Materials for Industrial Applications*; Kumar, K., Davim, J.P., Eds.; IGI Global: Hershey, PA, USA, 2018; pp. 297–331.
4. Sudagar, J.; Lian, J.; Sha, W. Electroless nickel, alloy, composite and nano coatings—A critical review. *J. Alloys Compd.* **2013**, *571*, 183–204. [CrossRef]
5. Lu, G.; Zangari, G. Study of the electroless deposition process of Ni-P-based ternary alloys. *J. Electrochem. Soc.* **2003**, *150*, C777–C786. [CrossRef]
6. Zhang, W.X.; Huang, N.; He, J.G.; Jiang, Z.H.; Jiang, Q.; Lian, J.S. Electroless deposition of Ni–W–P coating on AZ91D magnesium alloy. *Appl. Surf. Sci.* **2007**, *253*, 5116–5121. [CrossRef]
7. Balaraju, J.N.; Anandan, C.; Rajam, K.S. Morphological study of ternary Ni–Cu–P alloys by atomic force microscopy. *Appl. Surf. Sci.* **2005**, *250*, 88–97. [CrossRef]
8. Georgieva, J.; Armyanov, S. Electroless deposition and some properties of Ni–Cu–P and Ni–Sn–P coatings. *J. Solid State Electrochem.* **2007**, *11*, 869–876. [CrossRef]
9. Sankara Narayanan, T.S.N.; Selvakumar, S.; Stephen, A. Electroless Ni–Co–P ternary alloy deposits: Preparation and characteristics. *Surf. Coat. Technol.* **2003**, *172*, 298–307. [CrossRef]
10. Balaraju, J.N.; Rajam, K.S. Electroless deposition of Ni–Cu–P, Ni–W–P and Ni–W–Cu–P alloys. *Surf. Coat. Technol.* **2005**, *195*, 154–161. [CrossRef]
11. Balaraju, J.N.; Selvi, V.E.; Grips, V.W.; Rajam, K.S. Electrochemical studies on electroless ternary and quaternary Ni–P based alloys. *Electrochim. Acta* **2006**, *52*, 1064–1074. [CrossRef]
12. Balaraju, J.N.; Jahan, S.M.; Jain, A.; Rajam, K.S. Structure and phase transformation behavior of electroless Ni–P alloys containing tin and tungsten. *J. Alloys Compd.* **2007**, *436*, 319–327. [CrossRef]
13. Mukhopadhyay, A.; Barman, T.K.; Sahoo, P. Effect of heat treatment on microstructure and corrosion resistance of Ni-B-W-Mo coating deposited by electroless method. *Surf. Rev. Lett.* **2017**, *1950023*. [CrossRef]
14. Palaniappa, M.; Seshadri, S.K. Friction and wear behavior of electroless Ni–P and Ni–W–P alloy coatings. *Wear* **2008**, *265*, 735–740. [CrossRef]
15. Liu, H.; Lv, Y.Y.; Liu, Z.; Thompson, G.E. Dry sliding wear behaviour and structural characteristics of laser-annealed electroless Ni–P/Ni–Mo–P duplex coatings. *Tribol. Int.* **2016**, *103*, 343–351. [CrossRef]
16. Tien, S.K.; Duh, J.G. Thermal reliability of electroless Ni–P–W coating during the aging treatment. *Thin Solid Films* **2004**, *469*, 268–273. [CrossRef]
17. Mendoza, L.V.; Barba, A.; Bolarin, A.; Sanchez, F. Age hardening of Ni–P–Mo electroless deposit. *Surf. Eng.* **2006**, *22*, 58–62. [CrossRef]
18. Liu, H.; Yao, H.L.; Thompson, G.E.; Liu, Z.; Harrison, G. Correlation between structure and properties of annealed electroless Ni–W–P coatings. *Surf. Eng.* **2015**, *31*, 412–419. [CrossRef]
19. Liu, J.; Wang, X.; Tian, Z.; Yuan, M.; Ma, X. Effect of copper content on the properties of electroless Ni–Cu–P coatings prepared on magnesium alloys. *Appl. Surf. Sci.* **2015**, *356*, 289–293. [CrossRef]
20. Sharma, A.; Singh, A.K. Electroless Ni-P and Ni-P-Al_2O_3 nanocomposite coatings and their corrosion and wear resistance. *J. Mater. Eng. Perform.* **2013**, *22*, 176–183. [CrossRef]
21. Chen, W.; Gao, W.; He, Y. A novel electroless plating of Ni–P–TiO_2 nano-composite coatings. *Surf. Coat. Technol.* **2010**, *204*, 2493–2498. [CrossRef]
22. Farzaneh, A.; Mohammadi, M.; Ehteshamzadeh, M.; Mohammadi, F. Electrochemical and structural properties of electroless Ni–P–SiC nanocomposite coatings. *Appl. Surf. Sci.* **2013**, *276*, 697–704. [CrossRef]
23. Krishnaveni, K.; Sankara Narayanan, T.S.N.; Seshadri, S.K. Electroless Ni–B coatings: Preparation and evaluation of hardness and wear resistance. *Surf. Coat. Technol.* **2005**, *190*, 115–121. [CrossRef]
24. Balaraju, J.N.; Priyadarshi, A.; Kumar, V.; Manikandanath, N.T.; Kumar, P.P.; Ravisankar, B. Hardness and wear behaviour of electroless Ni–B coatings. *Mater. Sci. Technol.* **2016**, *32*, 1654–1665. [CrossRef]
25. Çelik, İ.; Karakan, M.; Bülbül, F. Investigation of structural and tribological properties of electroless Ni–B coated pure titanium. *Proc. IMechE Part J J. Eng. Tribol.* **2016**, *230*, 57–63. [CrossRef]

26. Dervos, C.T.; Novakovic, J.; Vassiliou, P. Vacuum heat treatment of electroless Ni–B coatings. *Mater. Lett.* **2004**, *58*, 619–623. [CrossRef]
27. Correa, E.; Zuleta, A.A.; Guerra, L.; Gómez, M.A.; Castaño, J.G.; Echeverría, F.; Liu, H.; Skeldon, P.; Thompson, G.E. Tribological behavior of electroless Ni–B coatings on magnesium and AZ91D alloy. *Wear* **2013**, *305*, 115–123. [CrossRef]
28. Aydeniz, A.I.; Göksenli, A.; Dil, G.; Muhaffel, F.; Calli, C.; Yüksel, B. Electroless Ni–B–W coatings for improving hardness, wear and corrosion resistance. *Mater. Technol.* **2013**, *47*, 803–806.
29. Serin, I.G.; Göksenli, A. Effect of annealing temperature on hardness and wear resistance of electroless Ni–B–Mo coatings. *Surf. Rev. Lett.* **2015**, *22*, 1550058. [CrossRef]
30. Ghaderi, M.; Rezagholizadeh, M.; Heidary, A.; Monirvaghefi, S.M. The effect of Al_2O_3 nanoparticles on tribological and corrosion behavior of electroless Ni–B–Al_2O_3 composite coating. *Prot. Met. Phys. Chem. Surf.* **2016**, *52*, 854–858. [CrossRef]
31. Rezagholizadeh, M.; Ghaderi, M.; Heidary, A.; Monirvaghefi, S.M. The effect of B_4C nanoparticles on the corrosion and tribological behavior of electroless Ni–B–B_4C composite coatings. *Surf. Eng. Appl. Electrochem.* **2015**, *51*, 18–24. [CrossRef]
32. Wan, Y.; Yu, Y.; Cao, L.; Zhang, M.; Gao, J.; Qi, C. Corrosion and tribological performance of PTFE-coated electroless nickel boron coatings. *Surf. Coat. Technol.* **2016**, *307*, 316–323. [CrossRef]
33. Riddle, Y.W.; Bailerare, T.O. Friction and wear reduction via an Ni–B electroless bath coating for metal alloys. *JOM* **2005**, *57*, 40–45. [CrossRef]
34. Bonin, L.; Vitry, V. Mechanical and wear characterization of electroless nickel mono and bilayers and high boron-mid phosphorus electroless nickel duplex coatings. *Surf. Coat. Technol.* **2016**, *307*, 957–962. [CrossRef]
35. Vitry, V.; Bonin, L. Formation and characterization of multilayers borohydride and hypophosphite reduced electroless nickel deposits. *Electrochim. Acta* **2017**, *243*, 7–17. [CrossRef]
36. Mukhopadhyay, A.; Barman, T.K.; Sahoo, P. Tribological behavior of sodium borohydride reduced electroless nickel alloy coatings at room and elevated temperatures. *Surf. Coat. Technol.* **2017**, *321*, 464–476. [CrossRef]
37. Mukhopadhyay, A.; Barman, T.K.; Sahoo, P. Effects of heat treatment on tribological behavior of electroless Ni–B coating at elevated temperatures. *Surf. Rev. Lett.* **2017**, *24* (Suppl. 1), 1850014. [CrossRef]
38. Mukhopadhyay, A.; Barman, T.K.; Sahoo, P. Tribological behavior of electroless Ni–B–W coating at room and elevated temperatures. *Proc. IMechE Part J J. Eng. Tribol.* **2018**. [CrossRef]
39. Mukhopadhyay, A.; Barman, T.K.; Sahoo, P. Effect of heat treatment on tribological behavior of electroless Ni–B–Mo coatings at different operating temperatures. *Silicon* **2018**, *10*, 1203–1215. [CrossRef]
40. Pal, S.; Sarkar, R.; Jayaram, V. Characterization of thermal stability and high-temperature tribological behavior of electroless Ni–B coating. *Metall. Mater. Trans. A* **2018**. [CrossRef]
41. Mukhopadhyay, A.; Barman, T.K.; Sahoo, P. Friction and wear performance of electroless Ni–B coatings at different operating temperatures. *Silicon* **2018**. [CrossRef]
42. Mukhopadhyay, A.; Barman, T.K.; Sahoo, P. Wear and friction characteristics of electroless Ni–B–W coatings at different operating temperatures. *Mater. Res. Express* **2018**, *5*, 026526. [CrossRef]
43. Mukhopadhyay, A.; Barman, T.K.; Sahoo, P. Tribological characteristics of electroless Ni–B–Mo coatings at different operating temperatures. *Surf. Rev. Lett.* **2018**, 1850175. [CrossRef]
44. Mattox, D.M. Film Characterization and Some Basic Film Properties. In *Handbook of Physical Vapor Deposition (PVD) Processing: Film Formation, Adhesion, Surface Preparation and Contamination Contro*; Mattox, D.M., Ed.; Noyes Publications: Westwood, NJ, USA, 1998; pp. 569–615.
45. Cai, F.; Huang, X.; Yang, Q. Mechanical properties, sliding wear and solid particle erosion behaviors of plasma enhanced magnetron sputtering CrSiCN coating systems. *Wear* **2015**, *324*, 27–35. [CrossRef]
46. Berg, G.; Friedrich, C.; Broszeit, E.; Berger, C. Development of chromium nitride coatings substituting titanium nitride. *Surf. Coat. Technol.* **1996**, *86*, 184–191. [CrossRef]
47. Zhen, J.; Zhu, S.; Cheng, J.; Qiao, Z.; Liu, W.; Yang, J. Effects of sliding speed and testing temperature on the tribological behavior of a nickel-alloy based solid-lubricating composite. *Wear* **2016**, *368*, 45–52. [CrossRef]